Indian Summer Monsoon Precipitation Climatology in a High-Resolution Regional Climate Model: Impacts of Convective Parameterization on Systematic Biases

P. MUKHOPADHYAY, S. TARAPHDAR, B. N. GOSWAMI, AND K. KRISHNAKUMAR

Indian Institute of Tropical Meteorology, Pune, India

(Manuscript received 17 June 2009, in final form 9 September 2009)

ABSTRACT

In an attempt to develop a better simulation of the climatology of monsoon precipitation in climate models, this paper investigates the impacts of different convective closures on systematic biases of an Indian monsoon precipitation climatology in a high-resolution regional climate model. For this purpose, the Weather Research Forecast (WRF) model is run at 45- and 15-km (two-way nested) resolution with three convective parameterization schemes, namely the Grell–Devenyi (GD), the Betts–Miller–Janjić (BMJ), and the Kain–Fritsch (KF), for the period 1 May–31 October 2001–07. The model is forced with the NCEP–NCAR reanalysis data as the initial and boundary conditions. The simulated June–September (JJAS) mean monsoon rainfall with the three convective schemes is compared with the observations. KF is found to have a high moist bias over the central and western coastal Indian region while GD shows the opposite. Among the three, BMJ is able to produce a reasonable mean monsoon pattern. In an attempt to get further insight into the seasonal bias and its evolution, the probability distribution function (PDF) of different rain-rate categories and their percentage contribution to the seasonal total are computed. BMJ and KF underestimate the observations for lighter rain rates and overestimate for rain-rate categories of more than 10 mm day^{-1}. GD shows an overestimation for lighter rain and an underestimation of PDF for moderate categories. The seasonal patterns of evolution of PDF plots of three rain-rate categories are analyzed to determine whether the convective schemes show any systematic bias throughout the season or if they have problems during certain phases of the monsoon. This shows that the GD systematically overestimates the lighter rain rate and underestimates the moderate rain rate throughout the season, whereas BMJ and KF have problems in the initial stages. The heavy rain category is systematically overestimated by the KF compared to the other two. To further evaluate the proportionate contribution of each rain-rate bin to the total rain, the percentage contribution of each rain rate to the seasonal total is computed. Analyzing all the rain-rate simulations produced by the three schemes, it is found that KF has a moist bias and GD has a dry bias in the spatiotemporal distribution of the monsoon precipitation. Further, this paper investigates the causes behind the mean monsoon precipitation bias. It is shown that GD produces a model climate where the vertical velocity is less than that of the observations up to 500 hPa and the vertically integrated moist instability is also weaker. KF, on the other hand, shows a higher than the observed vertical velocity and a stronger moist instability. Along with this, the vertical profile of heating suggests a warmer middle level in the KF case and significantly reduced midlevel heating for GD. Thus, KF (GD) has produced a model atmosphere that has a stronger (weaker) convective instability to produce the observed bias in the model precipitation. BMJ is found to simulate a reasonable heating profile, along with the realistic moist instability and seasonal cycle of evaporation and condensation. Insight derived from the analysis is expected to help improve the convective parameterizations.

1. Introduction

The prediction of seasonal mean Indian summer monsoon rainfall (ISMR) is very important for socioeconomic and water resource planning of the country of India. Also, projection of ISMR under different climate change scenarios is crucial for the planning of adaptation and mitigation strategies of the country. Unfortunately, today we have very little confidence in either the seasonal prediction of ISMR or its projections under climate change scenarios. Although the foundation for the predictability of the tropical climate has been laid (Charney and Shukla 1981; Shukla 1981), the skill in predicting the seasonal mean monsoon rainfall by almost all the global climate models remains limited (Kang et al.

Corresponding author address: Dr. P. Mukhopadhyay, Indian Institute of Tropical Meteorology, Dr. Homi Bhabha Rd., Pashan, Pune-411008, India.
E-mail: mpartha@tropmet.res.in

DOI: 10.1175/2009WAF2222320.1

2004; Kang and Shukla 2005; Kumar et al. 2005). Similarly, the intermodel variance of projections of ISMR by the models in the Fourth Assessment Report (AR4) of the Intergovernmental Panel on Climate Change (IPCC) is as large as the signal of increase in the ensemble means (Randall et al. 2007). Among a few other reasons, a major reason for the current suite of climate models' poor skill in predicting the seasonal mean ISMR and uncertainty in the projections under climate change scenarios is the large systematic dry bias over the Bay of Bengal (Randall et al. 2007).

Hence, a significant improvement in the simulation of the monsoon rainfall climatology in climate models is crucial for making any further progress toward seasonal prediction of ISMR or toward a reliable projection of it under the climate change scenarios. Resolving the regional heterogeneity in a high-resolution atmospheric general circulation model (AGCM) is one of the keys to improving the precipitation distribution over the region (Giorgi and Mearns 1991; Sperber et al. 1994; Jha et al. 2000; Rajendran and Kitoh 2008). However, running AGCMs at a resolution high enough to resolve the physiographical details (e.g., topography, mesoscale convection) requires significant computational resources. Thus, the computationally less expensive strategy of running regional climate models embedded in AGCMs has gained popularity (Dash et al. 2006; Im et al. 2006, 2008) when simulating regional climate at higher resolution since the mid-1990s.

A number of attempts have been made in the past to demonstrate the capability of regional models embedded in a GCM to simulate the Indian summer monsoon climatology (Bhaskaran et al. 1996; Jacob and Podzum 1997; Vernekar and Ji 1999; Lee and Suh 2000; Dash et al. 2006). The general conclusion of all these studies is that the regional models are able to show an improvement in the spatiotemporal distribution of monsoon rainfall, which is attributed to the increased resolution of these models. As the simulation of precipitation depends sensitively on the parameterization of convection in the model, it is important to identify the most suitable convective parameterization for a given high-resolution model to improve the simulation of the monsoon rainfall climatology.

Evaluations of the sensitivity of convective parameterization schemes on monsoon simulation have been performed in the past (Bhaskaran et al. 1996; Martin and Soman 2000; Das et al. 2001; Ratnam and Kumar 2005; Dash et al. 2006). Das et al. (2001) compared the July rainfall and monsoon circulation features using a T80 (~150 km horizontal resolution) global model with three different cumulus parameterization schemes. They inferred that the simplified Arakawa–Schubert (SAS) approach is able to produce realistic north–south and east–west rainfall distributions and circulation features compared to the other schemes. Ratnam and Kumar (2005) simulated two contrasting years of monsoon (1987 and 1988) by using the fifth-generation Pennsylvania State University–National Center for Atmospheric Research (Penn State–NCAR) Mesoscale Model (MM5) at 45-km resolution with a variety of cumulus parameterization schemes. They found that the Betts–Miller–Janjić (BMJ) and Kain–Fritsch (KF) schemes produced relatively better spatial distributions of the monsoon rainfall as compared to the Grell approach. Dash et al. (2006) used version 3 of the NCAR Regional Climate Model (RegCM3) to simulate the monsoon for 4 yr (1993–96) with a horizontal resolution of 55 km and showed that the Grell scheme is able to simulate the mean monsoon rainfall closer to the observation as compared to the Kuo approach. In all of the mentioned studies, it can be seen that the typical range of the horizontal resolutions used for the simulation of the Asian monsoon remains around 50 km. At this resolution, large-scale monsoonal features can be captured, but to resolve the physiographical heterogeneity and the mesoscale cloud clusters in the region, high-resolution regional climate models (RCMs) are required (Im et al. 2006, 2008). Giorgi et al. (1994), using a 60-km nested domain over the United States, showed that the simulated surface climatology appears to be realistic compared to the driving GCM. Jones et al. (1995) showed over Europe that the details of the simulated spatial distribution of precipitation, temperatures, etc. agree well with the observations using a finer-resolution RCM (e.g., a 50-km U.K. RCM), which is mainly attributed to the topography, coastline, and vegetation being better resolved. However, it remains to be seen whether the mean monsoon rainfall bias improves by using a high-resolution (less than 20 km) model that resolves the physiographical heterogeneity and mesoscale cloud clusters.

Therefore, the first objective of the present paper is to simulate the observed daily monsoon climatology over the Indian region at a high resolution using various cumulus parameterization schemes and its validation with available observed rainfall data. This can provide the needed high-resolution daily mean precipitation climatology of the Indian monsoon to assess the seasonal (June–September) biases arising due to possible shortcomings of different convective closures. Earlier, the RCM studies were mainly focused on the bias of seasonal (total) rain and did not offer any insights on how the bias is contributed by different categories of the simulated rain.

Therefore, the second objective of this paper is to bring out the biases in daily mean rainfall simulations arising from different rain-rate (light to heavy) categories. We believe this will help us to gain necessary insights about the contribution of different rain rates

toward the spatiotemporal bias of the seasonal total rainfall. A detailed investigation of this nature can also help in identifying the weaknesses in the formulation of moist convection, which can be improved further.

It may be worthwhile to mention here that in most of the earlier studies, simulation results, particularly precipitation, were merely compared with different cumulus schemes and conclusions were drawn about the inferiority or superiority of the schemes without providing many clues as to the possible sources of the bias. To gain sufficient insight into the further improvement of existing convective schemes and to reduce the uncertainties in the simulations, it is felt that a detailed understanding of the reasons behind the better performance of one or the other cumulus scheme is required. Therefore, the third objective of the paper is to investigate and identify the possible sources of biases in the simulation arising from different convective closures. Rajendran et al. (2002) showed that monsoon variability is sensitive to the heating rates arising from different cumulus parameterization schemes. It is also established that the large-scale monsoon circulation is mainly driven by the middle-tropospheric heating and large-scale organized convection. Thus, the apparent heat source plays a key role in maintaining the monsoonal convection. The evolution of convective instability during the season is another parameter that tells us about the strength of the organized convection. Detailed analyses of the apparent heat source and the moist static energy will reveal the thermodynamic structure of the simulated monsoon climate and bring out the strengths (weaknesses) of different convective closures in making the model atmosphere more unstable (less unstable) and moist (dry), thereby affecting the overall mean monsoon simulation.

In summary, this paper is intended to establish the bias in the mean monsoon simulation in general and the underlying spatiotemporal variability of the precipitation in particular and to diagnose further the possible source of the bias in the high-resolution model simulation. In the next section, the model, data, experimental design, and verification strategy are introduced, followed by results and discussion in section 3. Section 4 provides the conclusions of the study.

2. Model, data, experimental design, and verification

a. Model

The nonhydrostatic, fully compressible, terrain-following sigma coordinate mesoscale model Weather Research Forecast (WRF), version 2.2 (Skamarock et al. 2005), developed by NCAR, was used in the present study. The

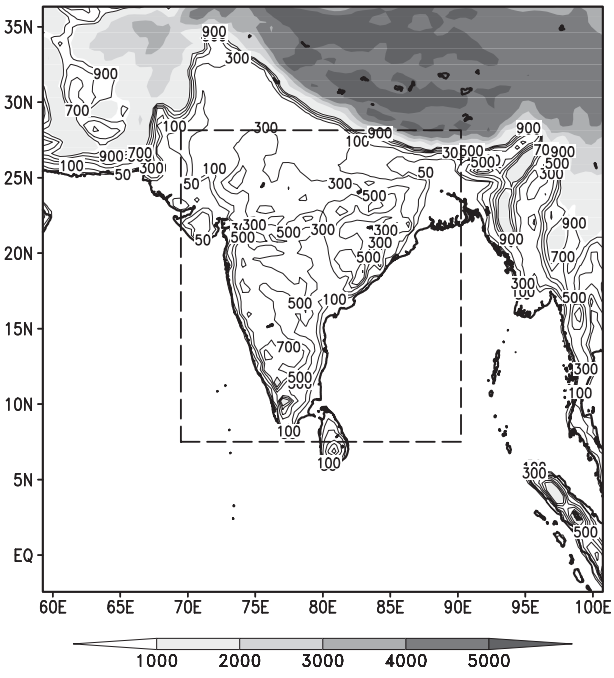

FIG. 1. WRF domain 100 × 100 (mother domain), at 45-km resolution, and nested domain 160 × 160, 15-km resolution. Model topography is contoured below 1000 m and shaded above.

model is used with two nested domains with horizontal resolutions of 45 and 15 km (Fig. 1) and 31 sigma levels with its top at 10 hPa. The model's mother domain covers the large-scale Indian monsoon region (2°S–37°N, 59°–101°E) with 100 grid points in the east–west and north–south directions. The nested domain focuses mainly on the Indian landmass (7°–27.5°N, 69°–91°E) with 160 grid points along the east–west and north–south axes. The model time steps were chosen to be 240 s.

The physical parameterization schemes used in the model are the microphysics scheme of Lin et al. (1983), the Monin–Obukhov (Monin and Obukhov, 1954) similarity scheme for the surface layer, the Yonsei University scheme for the PBL (Noh et al. 2003), the Rapid Radiative Transfer Model (RRTM) scheme for long waves (Mlawer et al. 1997), and the Dudhia (Dudhia 1989) scheme for short waves in all of the numerical experiments. Three convective parameterization schemes—namely Kain–Fritsch (KF; Kain and Fritsch 1993); Betts and Miller (1986), but modified further by Janjić (1994; BMJ); and Grell–Devenyi (GD; Grell and Devenyi 2002)—are used to simulate a 7-yr daily climatology of JJAS rainfall. These three schemes work within different closure frameworks; for example, KF uses the assumption of the removal of convective available potential energy (CAPE) in a grid column within an advective time. A trigger function based on the grid-resolved vertical motion is used to decide the time of activation of the scheme. The

resolvable-scale vertical motion is proportional to one-third to the power of the grid-resolved background vertical motion ($w^{1/3}$). If the upward motion is sufficiently large to overcome the convective inhibition, the scheme will activate (so long as the unstable layer is at least of 60-hPa depth). The advective precipitation is derived as a product of precipitation efficiency and the sum of the vertical fluxes of vapor and liquid at about 150–200 hPa above the lifting condensation level (Wang and Seaman 1997). For further details about the KF scheme formulation and its various features, readers are referred to a detailed studies by Kain and Fritsch (1993), Gallus (1999), Bechtold et al. (2001), and Kain (2004).

Unlike KF, the BMJ scheme includes deep and shallow convection and works based on the principle of relaxing the temperature and moisture profiles toward the reference environmental profile. The BMJ scheme essentially removes the conditional instability in each grid column by adjusting the vertical profile of the temperature and specific humidity toward the reference profile, which is derived based on the observations of Betts (1986) and Betts and Miller (1986). The scheme is triggered if a parcel when lifted moist adiabatically from the lower troposphere to a level above the cloud base, where it then became warmer than the environment. The GD is a cloud ensemble scheme. The unique aspect of the GD scheme is that it uses 16 ensemble members derived from five popular closure assumptions to obtain an ensemble-mean realization at a given time and location. The details of how to determine the ensemble mean can be found in Grell and Devenyi (2002). An ensemble approach is followed because statistically the ensemble members yield a large spread in the accumulated convective rainfall results.

b. Data and experiment

The regional model can be run with both initial and lateral boundary conditions (LBCs) from either global analysis data or the global model forecasts data. In our study, the mother domain simulations are driven by the National Centers for Environmental Prediction (NCEP)–NCAR reanalysis data at a resolution of 2.5° (Kalnay et al. 1996). The LBCs are updated every 6 h. RTG is a daily, high-resolution, real-time, global, sea surface temperature (SST) analysis (Thiebaux et al. 2003) that has been developed at the NCEP/Marine Modeling and Analysis Branch (MMAB). The daily SST product is produced on a ½° (latitude, longitude) grid, with a two-dimensional variational interpolation analysis of the most recent 24-h buoy and ship data, satellite-retrieved [*National Oceanic and Atmospheric Administration-17* (*NOAA-17*) Advanced Very High Resolution Radiometer (AVHRR)] SST data, and SSTs derived from satellite-observed sea ice coverage. The 6-hourly SSTs were obtained by linearly interpolating the daily SSTs of RTG and were used as the slowly varying lower boundary conditions for the model.

The model simulation spans from 1 May to 31 October for the years 2001–07 to study the seasonal (JJAS) mean rainfall for the 7-yr composite. The simulations corresponding to JJAS are used in the present study allowing 1 month as a model spinup time period. A 1-month spinup period is sufficient for the dynamical equilibrium between the lateral forcings and the internal physical dynamics of the model (Anthes et al. 1989). Three sets of simulations were used; the simulations were identical in all aspects except for their convective parameterization schemes, where we used BMJ, KF, and GD. A simple ensemble mean (ENS) of the above three sets of simulations is also computed for comparing the mean precipitation of each of these simulations. The model precipitation is stored every 6 h.

c. Verification strategy

The simulated model climatology in the mother domain for lower- (850 hPa) and upper-tropospheric (200 hPa) winds and the middle-tropospheric (500 hPa) temperature are compared with the European Centre for Medium-Range Weather Forecasts (ECMWF) interim reanalysis at a horizontal resolution of 1.5°. Subsequently, the daily precipitation simulated by the model (regridded at $1° \times 1°$ resolution) is compared with the daily gridded rainfall data from the India Meteorological Department (IMD) at $1° \times 1°$ resolution (Rajeevan et al. 2006) for the land areas and with the Global Precipitation Climatology Project (GPCP) and the Tropical Rainfall Measuring Mission (TRMM) rainfall data for the land–ocean area. The model precipitation biases are assessed by comparing the simulation results with the BMJ, KF, and GD schemes, and ENS with that of the gridded rainfall data of the IMD. To quantify the model deficiency in the spatiotemporal distribution of rainfall (over land only), the biases contributed from different rain-rate categories to the total rain are also computed. The sources of the model precipitation biases and deficiencies in different schemes are diagnosed with the vertical profiles of the apparent heat source (Q_1) and seasonal evolution of Q_1 and Q_2 based on Yanai et al. (1973) and compared with that derived from the ECMWF (interim) reanalysis data.

3. Results and discussion

a. The monsoon circulation and temperature pattern

We would like to begin the analysis with a 7-yr climatology of the lower- (850 hPa) and upper- (200 hPa)

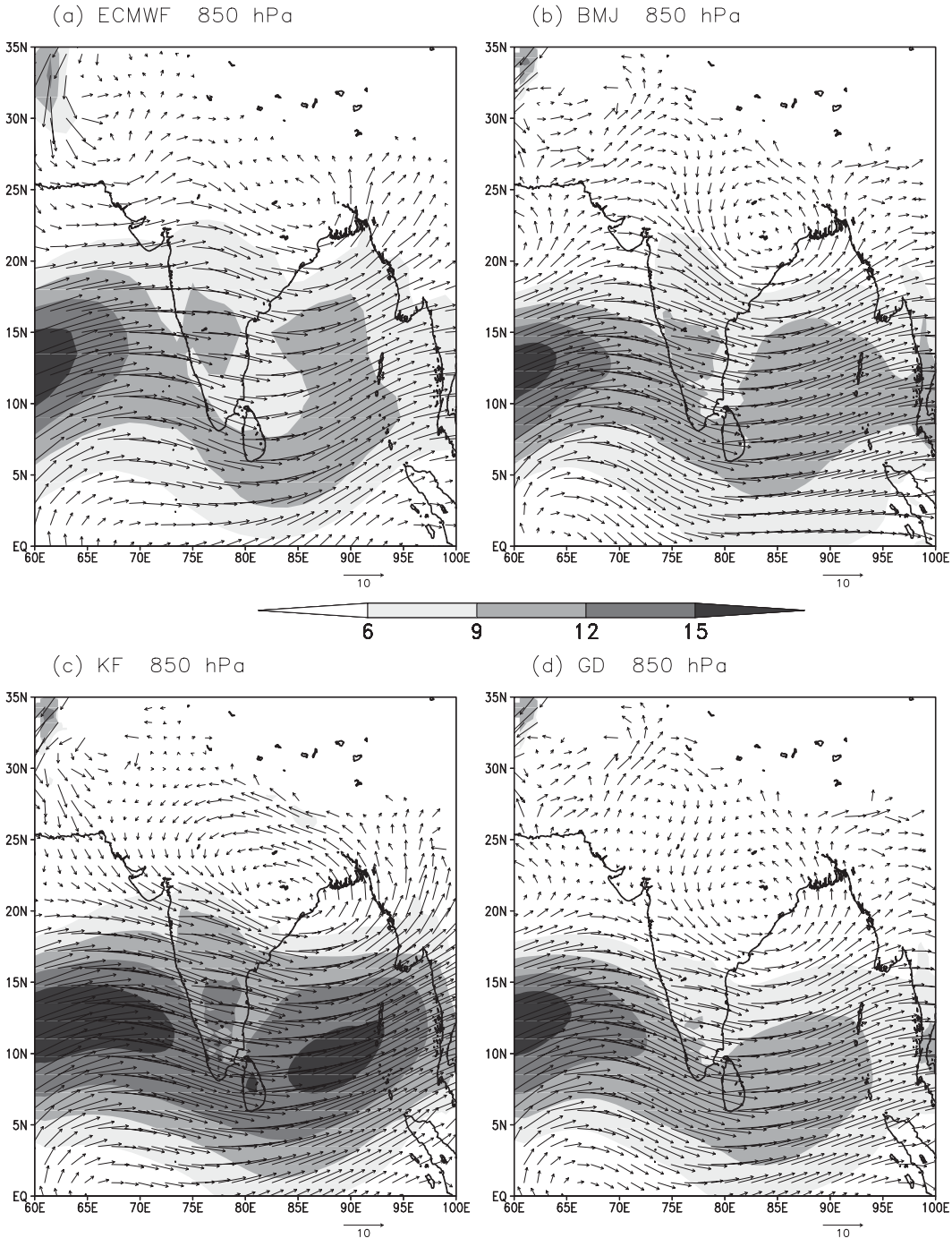

FIG. 2. JJAS-averaged mean 850-hPa winds (m s^{-1}) from (a) interim ECMWF reanalysis, (b) BMJ, (c) KF, and (d) GD for 2001–07; wind speeds above 6 m s^{-1} are shaded.

tropospheric wind fields for different convective schemes in the mother domain. It is important to examine whether the driving field in the mother domain is adequate for the nested domain (Im et al. 2006), particularly in connection with the synoptic-scale features of the Indian summer monsoon.

The JJAS mean winds (2001–07) at 850 and 200 hPa for each of the three schemes and from the ECMWF (observation) reanalysis are shown in Figs. 2 and 3, respectively. The large-scale southwesterly flow over the Arabian Sea (AS) and Bay of Bengal (BOB), and a cyclonic vorticity in the northern BOB, are broadly captured

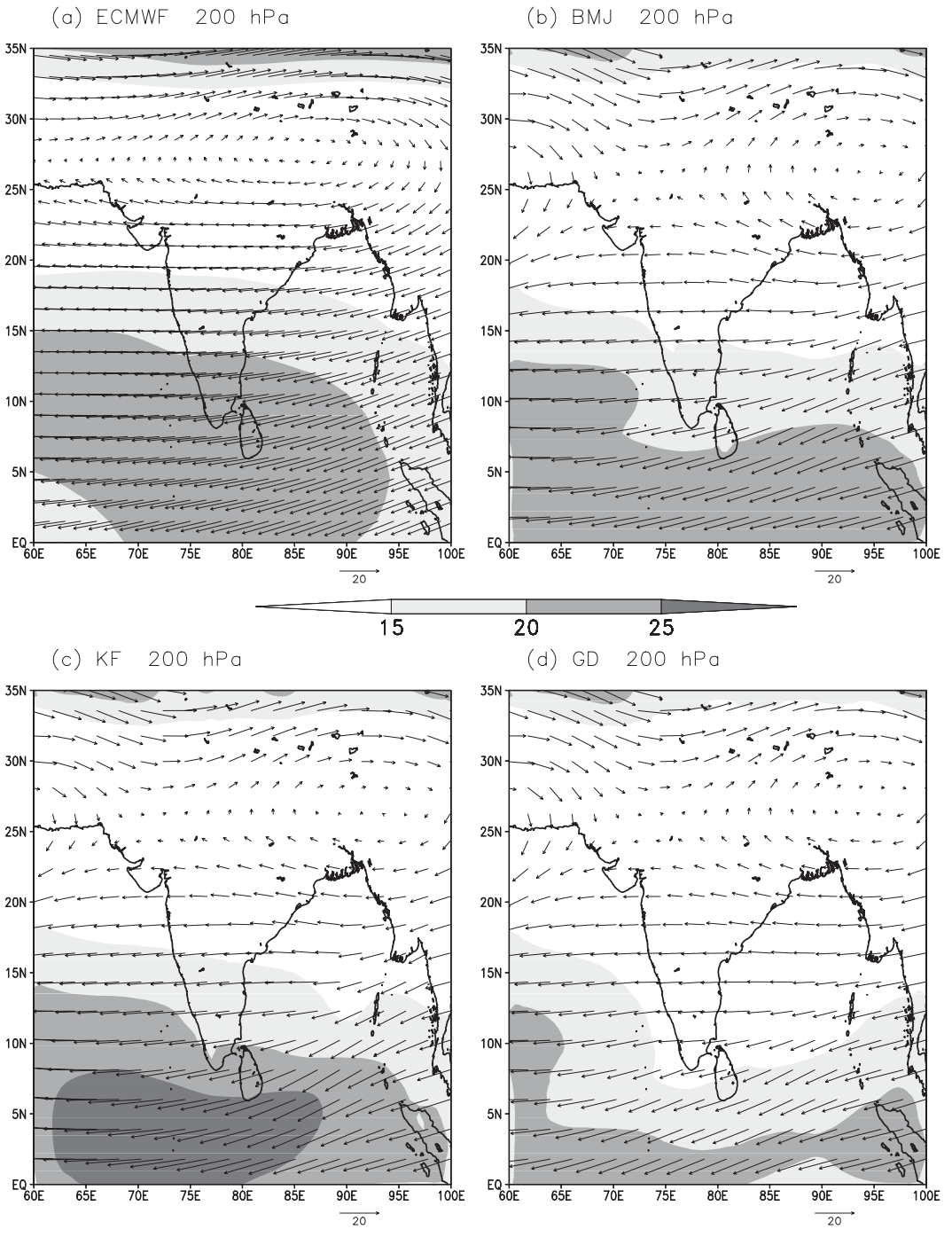

FIG. 3. As in Fig. 2, but for the 200-hPa level; wind speeds above 15 m s^{-1} are shaded.

by all three of the cumulus schemes (Figs. 2b–d) as compared to the observations (Fig. 2a). However, the low-level wind field (Fig. 2c) over the oceans appears to be stronger than the observations (Fig. 2a) in KF (RMSE of 3.76). The pattern correlation of 0.76 also suggests a disagreement between KF and the observations. The BMJ is found to show (Fig. 2b) a reasonable wind field, with a minimum RMSE of 3.09 and a maximum pattern correlation of 0.81 (Table 1) at the 850-hPa level. GD (Fig. 2d) has produced a weaker low-level wind field over the oceans (RMSE of 3.80; pattern correlation of 0.72).

The upper-level (200 hPa) easterly winds and the Tibetan anticyclone in the large scale are captured by all

TABLE 1. Pattern correlation and RMSE of the zonal wind at 850 and 200 hPa and temperature at 500 hPa by the BMJ, KF, and GD parameterizations.

	BMJ			KF			GD		
	U_{850}	U_{200}	T_{500}	U_{850}	U_{200}	T_{500}	U_{850}	U_{200}	T_{500}
Pattern correlation	0.81	0.97	0.83	0.76	0.96	0.83	0.72	0.96	0.82
RMSE	3.09	3.80	0.66	3.76	4.12	0.71	3.80	4.58	0.68

three of the experiments (Figs. 3b–d) but with varied levels of intensity. The center of the anticyclone is found to be shifted eastward in all three of the experiments compared to the observations. The ridge line is aligned with a tilt around 25°N. The simulated easterlies from KF along 5°N are found to be stronger (Fig. 3c) than those observed (Fig. 3a) as well as those simulated by the other two schemes (Figs. 3b and 3d). GD (Fig. 3d) simulates weaker easterlies in the south of the domain (Table 1). BMJ shows the most reasonable wind field at 200 hPa with the highest pattern correlation (0.97) and lowest RMSE (3.80).

From the above discussions it can be inferred that KF has simulated stronger low-level southwesterlies and corresponding cyclonic shear. GD, on the other hand, shows weaker than observed wind fields. However, BMJ is in better agreement with the observations over both of the seas (Table 1) as supported by the RMSE and pattern correlation. The middle-tropospheric (500 hPa) temperature distribution for the ECMWF reanalysis and the three convection schemes are also analyzed (figure not shown). This will bring out whether the model-simulated middle troposphere has a warmer or colder bias compared to the observations, which in turn can influence the instability of the simulated climate. The north–south temperature gradient with a maximum over Tibet is broadly captured by all the schemes. KF shows a warm bias over the central Indian region and has the highest RMSE (0.71; see Table 1), and BMJ shows a reasonable temperature gradient with the minimum RMSE (0.66) out of the three schemes.

b. Precipitation analyses

1) DISTRIBUTION OF MEAN MONSOON PRECIPITATION

The observed JJAS mean precipitation for 2001–07 over the Indian landmass from the IMD gridded (1° × 1°) dataset (Rajeevan et al. 2006) is shown in Fig. 4a. The same is done for land and oceanic areas from the TRMM and GPCP datasets and the results are shown in Figs. 4b and 4c, respectively. All of the datasets are regridded to 1° × 1° resolution for comparison. The later datasets have inherent limitations due to their smaller number of land stations and this is quite visible along the west coast region where the maximum difference is found with respect to IMD data. The IMD dataset is derived (Rajeevan et al. 2006) based on the data from 1803 stations that have at least 90% data availability. The model precipitation is brought to the same grid (1° × 1°) as that of the observations for validation. The JJAS mean precipitation amounts as obtained from BMJ, KF, GD, and ENS are shown, respectively, in Figs. 5a–d. The RMSEs (shaded) and biases of the mean precipitation (contour) over land in each simulation with respect to the (IMD) observations are shown in Figs. 6a–d. The RMSE of KF (Fig. 6b) is found to be maximal over central India and west coast of India compared to the other two schemes. The RMSE of GD appears (Fig. 6c) to be significantly less over the central Indian region and agrees well for this subregion with the ENS results (Fig. 6d). Although, the RMSE clearly shows the region of higher model error, it cannot answer the question of whether the model is over- or underestimating the precipitation in different subregions. To find an answer to this, the bias (Fig. 6; contour) is further analyzed. The BMJ shows (Fig. 6a) a positive bias over western and central India, while a dry bias is confined over the eastern region near the foothills of the Himalaya. The spatial pattern of dry and moist biases in the KF scheme (Fig. 6b) is very similar to that of BMJ (Fig. 6a). However, the wet bias simulated by KF is much larger than that simulated by BMJ. The GD scheme, on the other hand, shows (Fig. 6c) a drier bias over the whole country with the exception of a small pocket over the southwestern peninsula. This analysis, however, neither brings out the reasons behind such a spatial distribution of the biases, nor does it throw any light on how the bias in the seasonal total is evolving from the contributions of various rain-rate categories. The ENS (Fig. 6d) shows a distribution of moist and dry biases that is qualitatively similar to that of BMJ (Fig. 6b) but with a substantial reduction in the west coast bias.

The model's ability to simulate the evolution of the climatological mean seasonal cycle of precipitation and the climatological intraseasonal oscillation (CISO) of the Indian monsoon (2001–07 composite) are examined in Fig. 7. The time evolution of the daily climatological mean precipitation simulated by the models averaged over 70°–90°E as a function of latitude (Figs. 7b–d) is compared with that from the observations (IMD; see Fig. 7a). The seasonal cycle and the northward propagation are found to be reasonably simulated in BMJ (Fig. 7b) within certain epochs, whereas KF too frequently shows intraseasonal oscillations with (Fig. 7c) stronger magnitude and precipitation that appear to be stagnated at around 21°N. From the above analyses, it appears that BMJ is able to reproduce spatial and

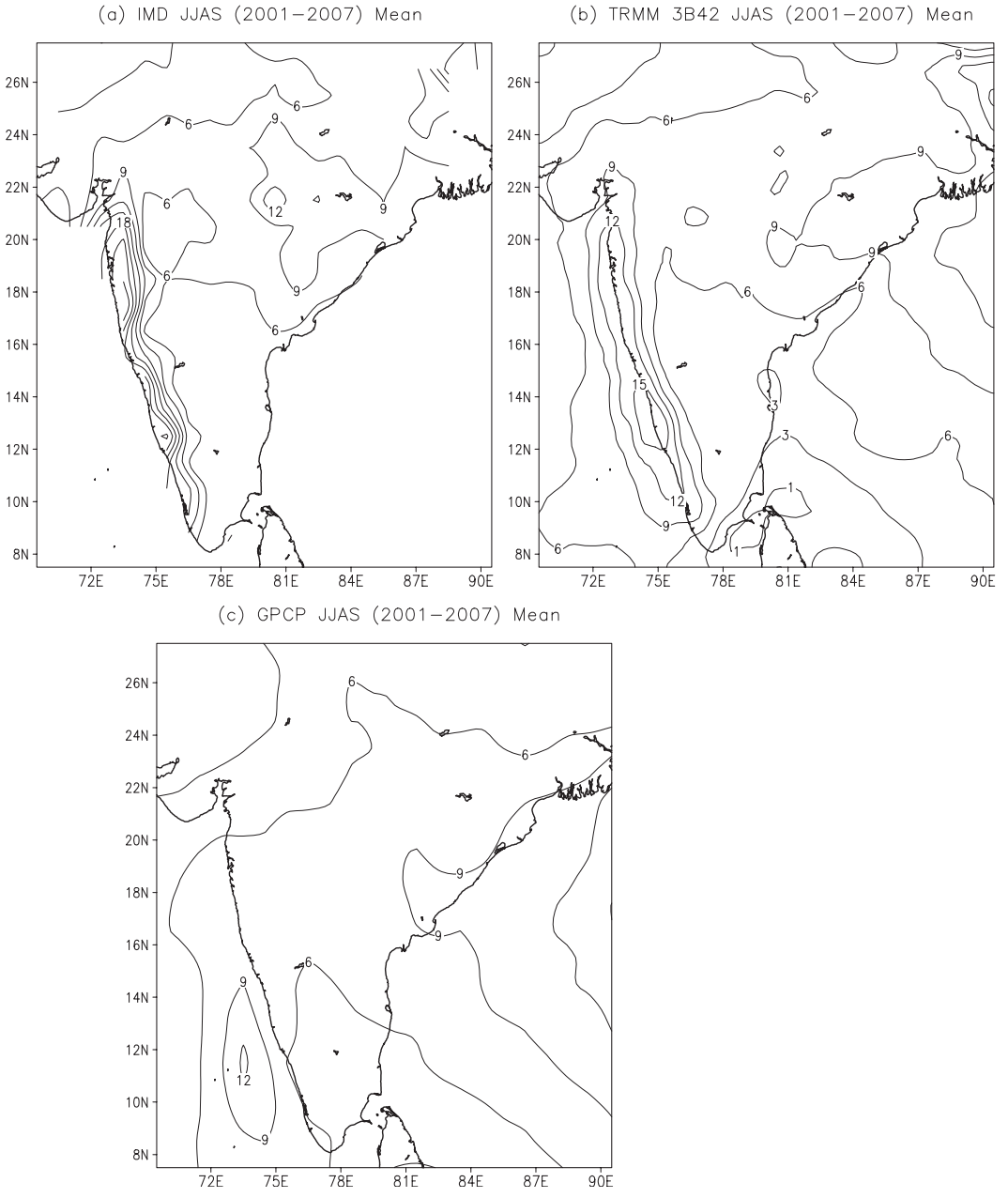

FIG. 4. JJAS-averaged mean surface precipitation (mm day^{-1}) from (a) IMD, (b) TRMM 3b42, and (c) GPCP for 2001–07.

temporal precipitation features that are closer to the observations as compared to other schemes.

2) SYSTEMATIC ERROR IN SIMULATED PRECIPITATION DISTRIBUTION

To investigate the spatiotemporal variability of precipitation superimposed on the seasonal mean, daily mean rainfall probability distribution functions (PDFs) are computed for different ranges of rain rates (Fig. 8). The PDFs are constructed by binning the daily mean rainfall amount for each grid point in 1 mm day^{-1} bins and expressed in percentages considering only the rainy grid cells over land areas for the season (JJAS) as a whole (DeMott et al. 2007). This brings out whether a particular rain rate is occurring more (less) frequently with respect to the observed PDF. The PDF plot indicates that BMJ and KF underestimate the observations of lighter rain rates and overestimates the rain-rate

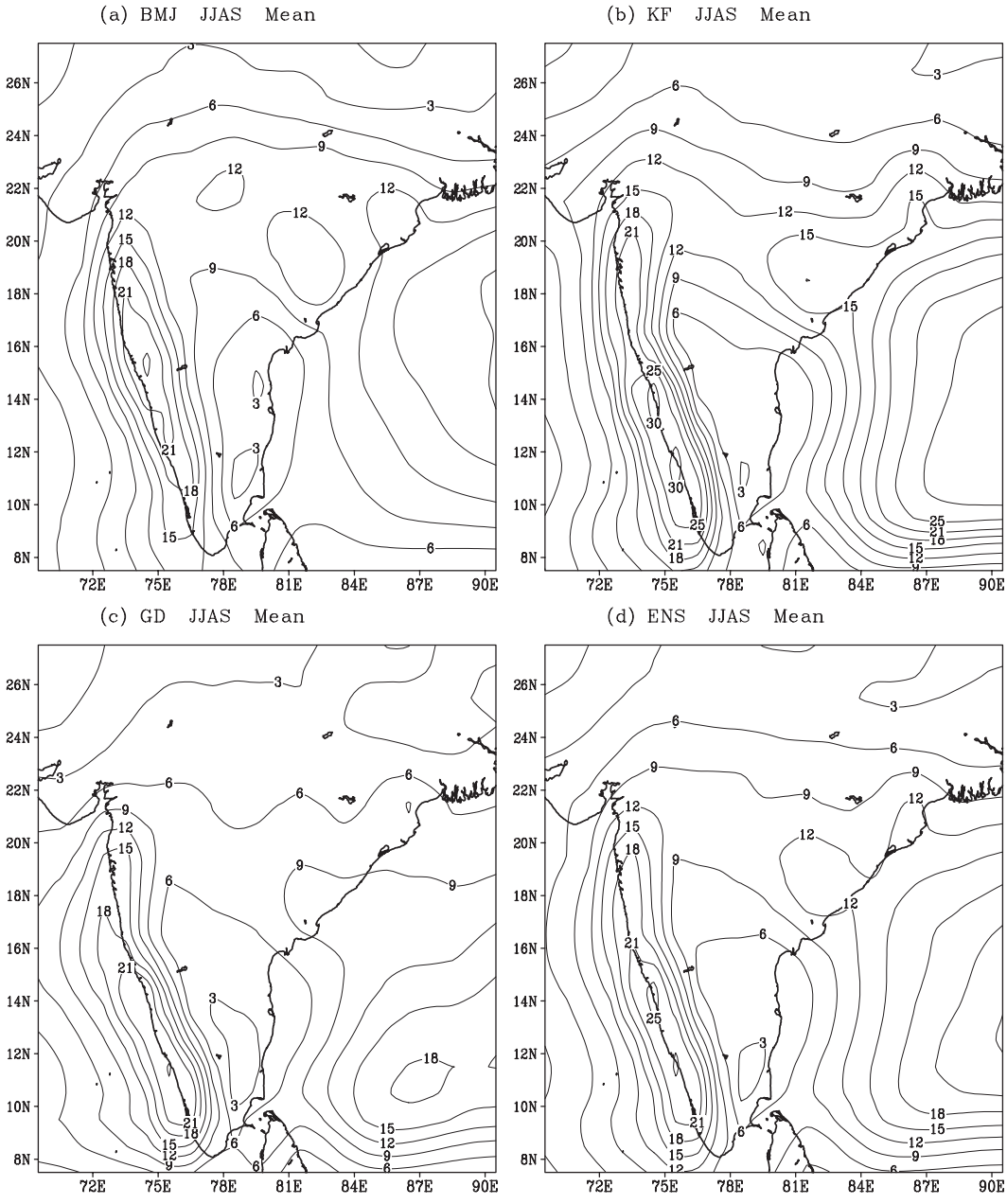

FIG. 5. As in Fig. 4, but for (a) BMJ, (b) KF, (c) GD, and (d) ENS.

categories of more than 10 mm day^{-1}. GD, on the other hand, shows a mixed distribution with the PDF being higher than the observations for lighter rain rates and an underestimation in the middle category (10–40 mm day^{-1}) and thereafter showing an overestimation. The question that can be raised now is whether the schemes systematically show higher or lower biases for certain rain-rate categories throughout the season, or do they have problems in capturing certain phases of the monsoon. To answer this, three rain-rate categories are chosen: less than 10 mm day^{-1} (light), between 10 and 40 mm day^{-1} (moderate), and more than 40 mm day^{-1} (heavy). This classification is made because the PDFs for all the schemes (Fig. 8) show a marked difference at the above-mentioned threshold rain rates.

The temporal evolution of the PDF as represented by the three above-mentioned rain-rate categories is shown in Fig. 9. Time evolution of GD (for light rain rate) shows (Fig. 9a, dot–dash) an overestimation of the PDFs throughout the season compared to the observations.

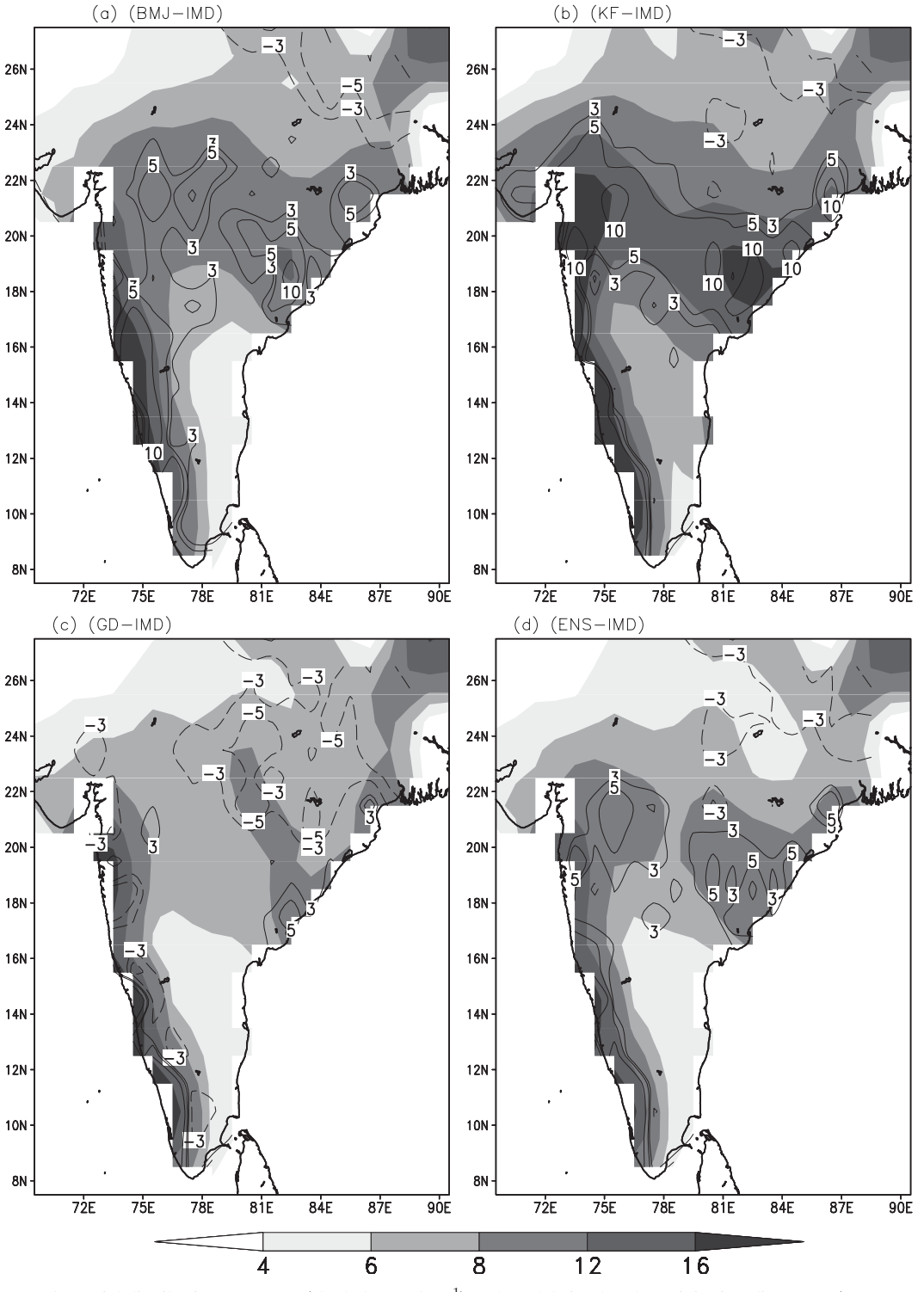

FIG. 6. Spatial distribution of RMSE (shaded; mm day^{-1}) and model-simulated precipitation difference (contour; mm day^{-1}) of (a) BMJ, (b) KF, (c) GD, and (d) ENS from IMD observations.

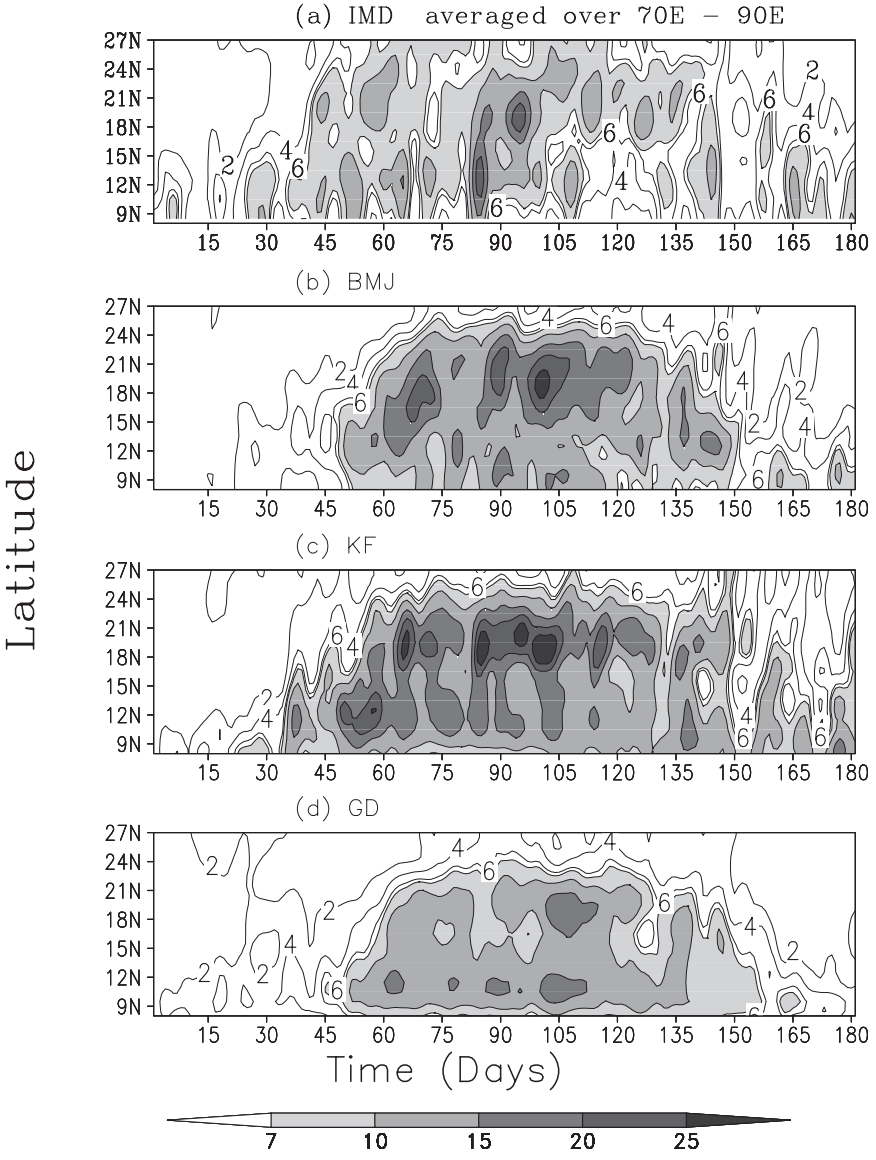

FIG. 7. Latitude–time cross sections of daily mean precipitation averaged over 70°–90°E from May to October 2001–07 from (a) IMD, (b) BMJ, (c) KF, and (d) GD.

BMJ (light rain rate) shows (Fig. 9a, long dash) an overestimation of PDFs in the beginning (first 30 days) of the season but is in good agreement with the observations for the remaining season. The PDFs of KF (Fig. 9a; dots) in the light rain-rate category are found to be similar to those of BMJ. For a moderate rain rate, GD (Fig. 9b) has systematically underestimated the observed PDFs throughout the season. For the heavy rain-rate category, KF shows a systematic bias of overestimation all through the season (Fig. 9c). Thus, from the PDF distribution, it appears that the GD has a systematic bias in producing underestimation (overestimation) of moderate (lighter) rain-rate categories throughout the season. BMJ has a prominent bias in the beginning of the season for all the categories. KF shows a significant overestimation for the heavy rain-rate category throughout the season. It is also found that the heavy precipitation (40 mm day^{-1}) PDF has a lag of ~15 days for BMJ and GD as compared to the observations and also KF. To find an answer to this model anomaly, for BMJ and KF we hypothesize that the large-scale moisture transport from the Arabian Sea could be the cause as it is seen to happen mostly in the beginning of the season. To verify this, we have chosen an area (extending from 7°–17°N, 60°–75°E) over the Arabian Sea and computed the time evolution of the area-averaged moisture transport at the 850-hPa level

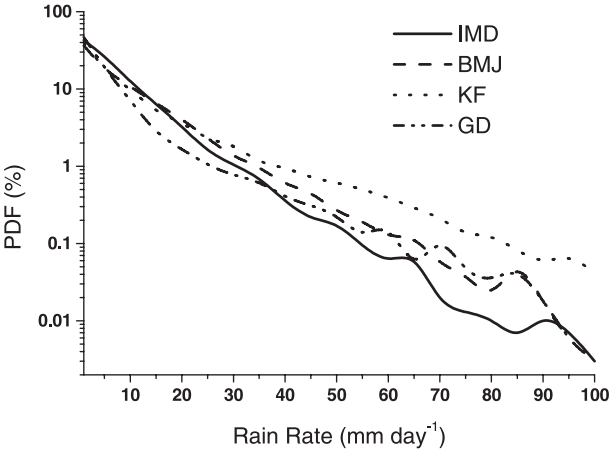

FIG. 8. Time- (JJAS) averaged daily mean rainfall rate probability distributions (%) from IMD (solid line), BMJ (dashed), KF (dotted), and GD (dotted–dashed) for 2001–07 over the inner domain.

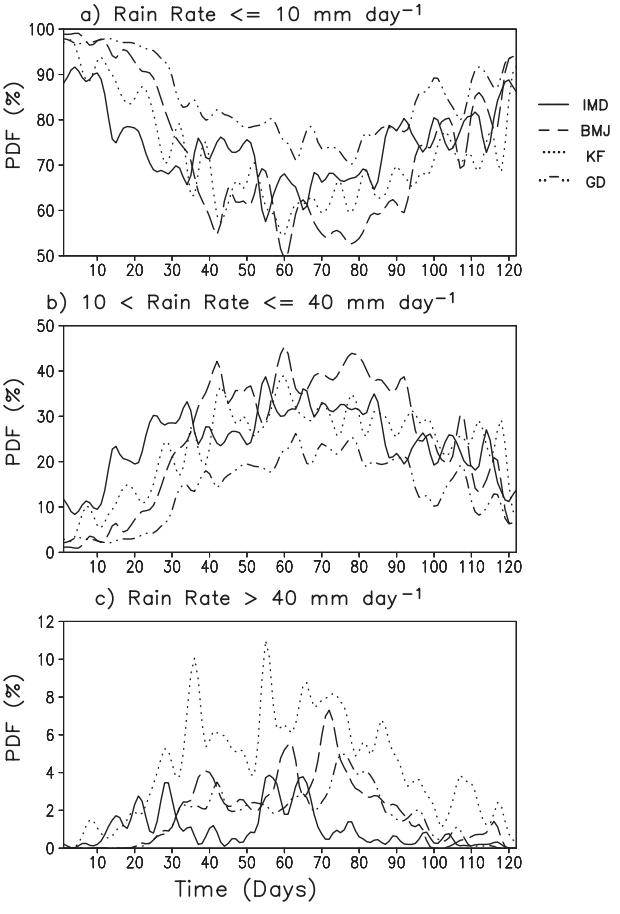

FIG. 9. Seasonal evolution (JJAS) of daily mean rainfall rate probability distributions (%) from IMD (solid line), BMJ (dashed), KF (dotted), and GD (dotted–dashed) for 2001–07 in rain rates (a) $\leq$10 mm day^{-1}, (b) 10 $<$ rain rate $\leq$ 40 mm day^{-1}, and (c) $>$40 mm day^{-1}.

(figure not shown). It is quite noticeable that, the moisture transport is significantly higher for the observation and also for the KF in the initial stages; however, in the BMJ and GD cases, it builds up late in the simulated climate.

At this point, it may be relevant to evaluate the proportionate contribution of each rain-rate bin to the total rain, which will bring out the overall percentage share of each rain rate to the total rain. The contributions of each rain-rate bin to the total rain, along with the PDF distribution (Figs. 8 and 9), can establish the bias arising from the frequency distribution as well as from the proportionate quantity of each rain rate. To address this, the percentage contributions of each rain rate to the total (JJAS) rain are shown in Fig. 10 for each of the three schemes and for the observations.

While the contribution from the rain-rate categories higher than 40 mm day^{-1} simulated by GD is close to the observations, the light rain categories simulated by this method contribute much higher amounts to the total than was observed (Fig. 10, dot–dash). On the other hand, intermediate categories of rain simulated by GD makes much smaller contributions to the total than observed. The contribution to the total by different rain categories simulated by the KF scheme, however, is such that (Fig. 10, dots) the rain-rate bin of 0–25 mm day^{-1} makes a smaller contribution than was observed while the rain rates higher than 25 mm day^{-1} make a substantially higher percentage contribution to the total than was observed. The BMJ scheme (long dash) appears to produce the closest possible contribution among the three for all of the rain-rate categories. The moist (dry) bias in simulating the seasonal total rainfall pattern by KF (GD) (Figs. 6b and 6c) is related to the biases in simulating different rain-rate categories by the two schemes (Fig. 10).

It is clear from the above analyses (Figs. 8–10) that GD has a systematically high bias in the lighter rain-rate categories and a low bias for medium rain-rate categories. These two contrasting biases tend to cancel each other, so that the seasonal mean spatial rainfall distribution appears fairly realistic (Fig. 6c) over the central Indian region. The above analyses indicate that the amount and frequency of light to moderate rain-rate categories are simulated with certain biases. This will significantly affect the performance of the monsoon simulation. The errors in the PDFs of simulated rainfall at different rain-rate thresholds and inaccurate percentage contribution will eventually decide the dry or moist biases of precipitation over the domain, as seen in GD (Fig. 6c).

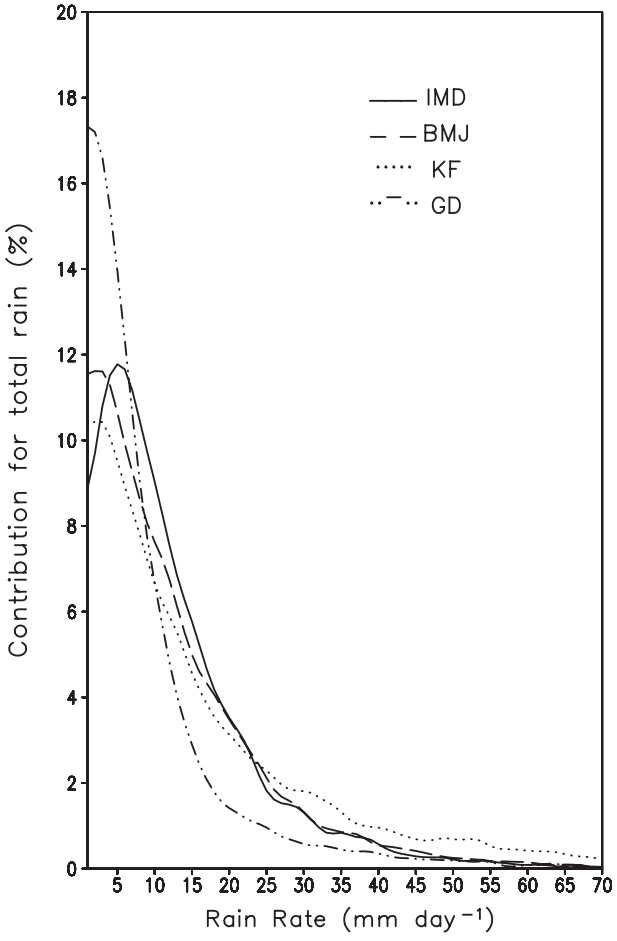

FIG. 10. As in Fig. 8, but for the contribution to the total seasonal rainfall (%) as a function of rain rate.

The spatial distribution of the percentage rainy days for different rain-rate categories (light, moderate, and heavy) for the season as a whole is shown in Fig. 11. The top panel in Fig. 11 brings out the spatial biases in simulating the rainy days for each scheme under the lighter rain-rate category. The observations (Fig. 11a) show 30%–40% rainy days for the lighter rain-rate category over parts of the southern peninsula and central India. GD grossly overestimates this over the whole country. BMJ shows (Fig. 11b) a reasonable percentage of rainy days over central and southern India but overestimates it in the northern and eastern parts of the country. The rainy days simulated by KF are similar to that simulated by BMJ.

In the moderate rain-rate category, BMJ shows (Fig. 11f) a moist bias east of the Western Ghats and in some pockets along the east coast. KF produces a moist bias over the east coast but reproduces the relatively drier area east of the Western Ghats. The GD scheme has a significant dry bias in the moderate category showing a smaller percentage of rainy days over central India and its surrounding region. In the heavy rain-rate category (Fig. 11, bottom), KF is found to have a substantial bias along the west coast as well as over major parts of central India. Thus, the spatial distributions of the percentages of rainy days are able to bring out the reasons behind the moist bias in central India by KF and the dry bias by GD, which is seen in Fig. 6.

After establishing the spatiotemporal biases in different rain-rate categories arising from different convective schemes, the question arises as to what is causing these deficiencies. The physical and thermodynamical causes of the above-mentioned biases and deficiencies will be evaluated further in the subsequent sections.

c. *Sources of bias*

The domain-averaged (5°–35°N, 60°–100°E) vertical velocity for JJAS composited for the 7 yr is shown in Fig. 12a and compared with the ECMWF reanalysis. The large-scale vertical velocity during monsoon regime represents the large-scale weak ascent that prevails over the country and its manifestation can be seen in the dominance of lighter rainfall of stratiform nature (Schumacher and Houze 2003). The simulated vertical velocity shows that KF substantially overestimates the observations throughout the troposphere whereas BMJ and GD underestimate up them to the 500-hPa level. Thus, BMJ and GD have large-scale ascents that are less than what was observed in the simulated climate in the lower troposphere. The overestimation of the large-scale ascent by KF may be manifested in its tendency for a moist bias in the lighter rain-rate categories. Similar results were reported by Bhaskaran et al. (1996) for RCM simulations over the Indian region. These variations in vertical velocity, as well as precipitation, appear to be driven by the tropospheric heating (Bhaskaran et al. 1996). To establish the moist bias of the schemes, the vertically integrated (950–150 hPa) moist static energy (MSE) result is averaged over the whole domain composited for 7 yr are plotted for each of the schemes (BMJ, KF, and GD; see Fig. 12b) for the JJAS. It is interesting to note that the seasonal cycle of gradual increase in MSE from the monsoon onset till its withdrawal is broadly captured by all three of the schemes. However, the amount of instability is higher in KF as compared to in BMJ and GD, while GD shows a weaker moist instability, particularly at the time of the peak monsoon. BMJ lies in between KF and GD. Thus, from the moist instability angle also, KF (GD) seems to produce a more (less) convectively unstable model climate.

To address the issue of tropospheric heating as a cause of model precipitation biases, the apparent heat source (Q_1) and moisture sink (Q_2) are evaluated. Here, Q_1 and

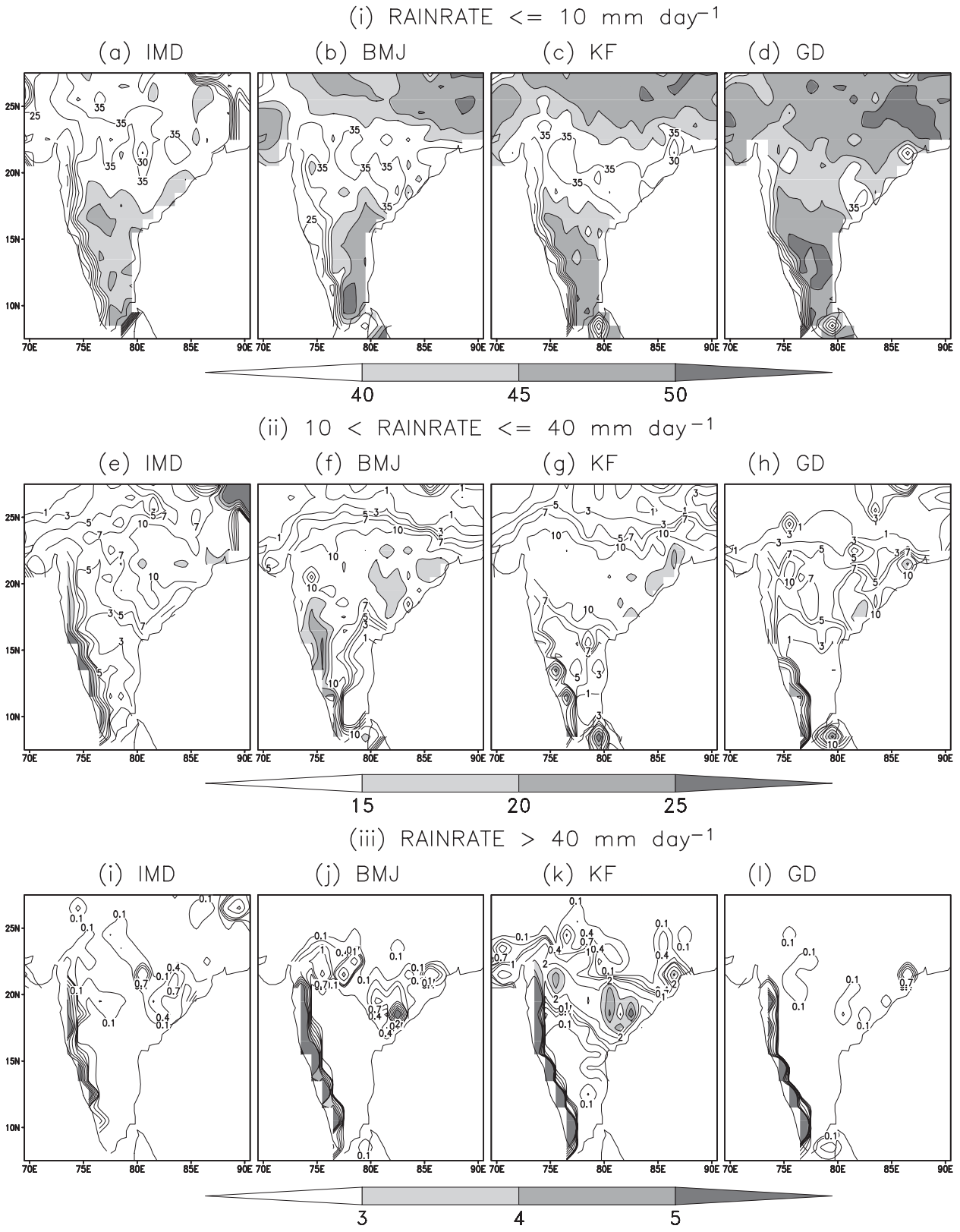

FIG. 11. Time- (JJAS) averaged spatial distributions of the percentage of rainy days with respect to the total number of rainy days from (a) IMD, (b) BMJ, (c) KF, and (d) GD for 2001–07 in rain rates (i) ≤10 mm day^{-1}, (ii) 10 < rain rate ≤ 40 mm day^{-1}, and (iii) >40 mm day^{-1}.

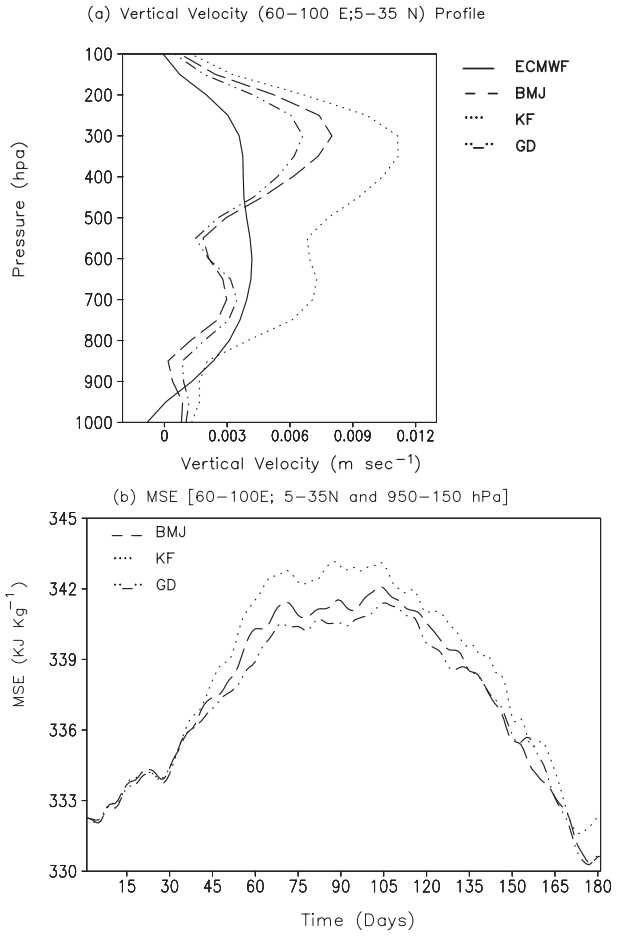

FIG. 12. Time- (JJAS) and domain-averaged (5°–35°N, 60°–100°E) (a) vertical velocity (m s^{-1}) profiles from ECMWF (solid line), BMJ (dashed), KF (dotted), and GD (dotted–dashed), and (b) the time evolution (May–October) of MSE (KJ kg^{-1}) vertically integrated between 950 and 150 hPa, for 2001–07.

Q_2 (Yanai et al. 1973) compare the collective effects of convection on the large-scale thermodynamics. The expressions for Q_1 and Q_2 are

$$Q_1 = C_p\left(\frac{p}{p_0}\right)^k\left(\frac{\partial\theta}{\partial t} + \mathbf{V}\cdot\nabla\theta + \omega\frac{\partial\theta}{\partial p}\right) \tag{1}$$

and

$$Q_2 = -L\left(\frac{\partial q}{\partial t} + \mathbf{V}\cdot\nabla q + \omega\frac{\partial q}{\partial p}\right), \tag{2}$$

where θ is the potential temperature, q is the mixing ratio of water vapor, $\mathbf{V}$ is the horizontal velocity, ω is the vertical velocity, and p is the pressure. In Eq. (1), $\kappa = R/C_p$, where R and C_p are, respectively, the gas constant and the specific heat at constant pressure of dry air; $p_0 = 1000$ hPa; L is the latent heat of condensation; and ∇ is the isobaric gradient operator.

As mentioned in Liu and Moncrieff (2007, hereafter LM07), Q_1 is the sum of the latent heating associated with phase changes, the vertical eddy transport, the subgrid diffusion that includes the divergence of the surface sensible heat flux, and the radiative heating. Similarly, Q_2 comprises the net condensation, the vertical eddy transport of moisture, and the subgrid mixing. As in our experiment (similar to LM07), the archived model output contains the atmospheric variables and does not include the variables of the microphysical processes and subgrid diffusion, Q_1 and Q_2 are estimated from the thermodynamic conservation equations by horizontally averaging over the outer domain using Eqs. (1) and (2).

Further, vertical integration of Eqs. (1) and (2) in the total atmospheric column gives

$$\langle Q_1\rangle = \langle Q_R\rangle + LP + S \tag{3}$$

and

$$\langle Q_2\rangle = L(P - E), \tag{4}$$

where Q_R is the radiative heating rate, P is the precipitation rate, S is the sensible heat flux, and E is the evaporation rate. The bracketed quantity means the vertical integration from 950 to 150 hPa.

As the monsoon convection is predominantly driven by the large-scale distribution of heat (Xavier et al. 2007), the vertical distribution of Q_1 is shown in Fig. 13 and compared with the ECMWF analysis. The midlevel heating is hardly present (Fig. 13, dot–dash) in GD whereas KF (dots) has produced a significantly stronger heating in the middle troposphere. The Q_1 profile of BMJ (dashed) lies in between KF and GD. The profile obtained from BMJ is reasonably comparable with that of the ECMWF reanalysis. Underestimation (overestimation) of Q_1 by GD essentially can cause a weaker (stronger) instability (KF) and may lead to weaker (more intense) convection for these schemes.

After identifying the bias in the JJAS-averaged vertical structure of the heat source by each scheme, our study will be incomplete if the climatological evolutions of Q_1 and Q_2 are not examined. The seasonal evolutions of Q_1 and Q_2 will help us in terms of understanding the deficiencies in the convection schemes more clearly. Xavier et al. (2007) showed that during winter and spring Q_2 is negative and it increases slowly, suggesting a stronger evaporation than precipitation during this time. Soon after the onset of the monsoon, Q_2 starts to increase at a faster rate, but the evaporation continues to dominate because of the warm landmass and about two

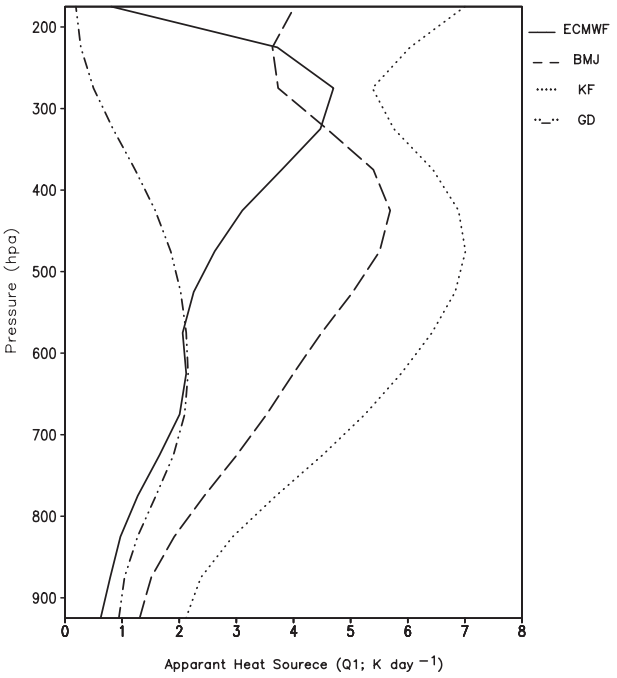

FIG. 13. Time- (JJAS) and domain-averaged (5°–35°N, 60°–100°E) vertical profiles of the apparent heat source (K day^{-1}) from BMJ (dashed), KF (dotted), ECMWF (solid), and GD (dotted–dashed) for 2001–07.

pentads after the onset, precipitation overcomes evaporation. So the moisture sink is not a leading process during the onset or at the time the Indian summer monsoon is set up. A remarkable feature is the cancellation between the heat source and the adiabatic cooling during the monsoon months (JJAS). However, the significant temperature increase that is observed during the premonsoon period arises largely from the adiabatic warming, sensible heating over the Tibetan Plateau, and vertical mixing. In the case of withdrawal of the monsoon, there is a coherent pattern of the evolution of the climatological values of Q_1 and Q_2. The seasonal evolutions of Q_1 and Q_2 are well brought out by the ECMWF (interim) reanalysis (Fig. 14a). Keeping this observational analysis in the mind, seasonal evolutions of Q_1 and Q_2 are shown in Figs. 14a–d and compared with that of the ECMWF analysis. The domination of evaporation (Q_2) compared to precipitation (Q_1) until mid-June is prominently captured (Figs. 14b and 14c) by BMJ and KF. The enhancement of condensation (precipitation) overcoming evaporation after the monsoon onset and followed by a maxima in July–August and the reduction in precipitation at the time of withdrawal are reasonably captured only by BMJ. KF could not show the reduction in precipitation and the enhancement of the evaporation at the time of withdrawal and as a result precipitation is found to dominate during the majority of the season. This can be attributed to the high moist bias in the spatiotemporal distribution of precipitation by KF. GD (Fig. 14d) has hardly reproduced the seasonal variabilities of the evaporation and precipitation, and both processes are found to be comparable to each other throughout the season, which is unrealistic as per the observations. The weak evolutions of Q_1 and Q_2 can be attributed to the dry bias shown by GD in the seasonal mean precipitation.

4. Conclusions

The precipitation climatology at a high level of resolution (15 km) for a period of 7 yr is prepared by running WRF from May to October for each year over the Indian region. The sensitivity levels of three cumulus parameterization schemes are evaluated in simulating the spatiotemporal evolution of the Indian summer monsoon (ISM). The seasonal bias of the mean monsoon rainfall is determined with respect to observed rainfall data over the Indian landmass from IMD. Comparing the three convective parameterization schemes, KF is found to have a high moist bias over central India as well as along with the west coast in the seasonal mean. GD apparently shows a dry bias over the central and eastern parts of the Indian region. BMJ, on the other hand, is found to produce a moist bias over the central Indian region.

PDFs of different rain-rate categories and their percentage contributions to the total seasonal rain are investigated as they play an important role in determining the overall model bias. These analyses also show that GD systematically overestimates the lighter rain-rate category and underestimates the moderate category throughout the season. On the other hand, KF significantly overestimates the heavy rain-rate category throughout the season. Among the three, BMJ produces a PDF of precipitation that is closest to the observations for all of the rain-rate categories. The higher percentage contribution by KF from the rain-rate bins of 25 mm day^{-1} or more, along with significant overestimation of the observed PDF in the high rain-rate category, can be responsible for the positive bias seen in the spatial plot of the seasonal mean precipitation. The reasonably good simulation of seasonal mean rainfall by GD over central India (Fig. 6c) appears to be due to the cancellation of two contrasting biases in simulating the different rain-rate categories, namely overestimation of low rain-rate categories and underestimation of moderate rain-rate categories. BMJ is able to produce a reasonable bias out of the three.

After identifying the details of the biases for each convection scheme arising from different rain-rate categories and their manifestations on the spatiotemporal

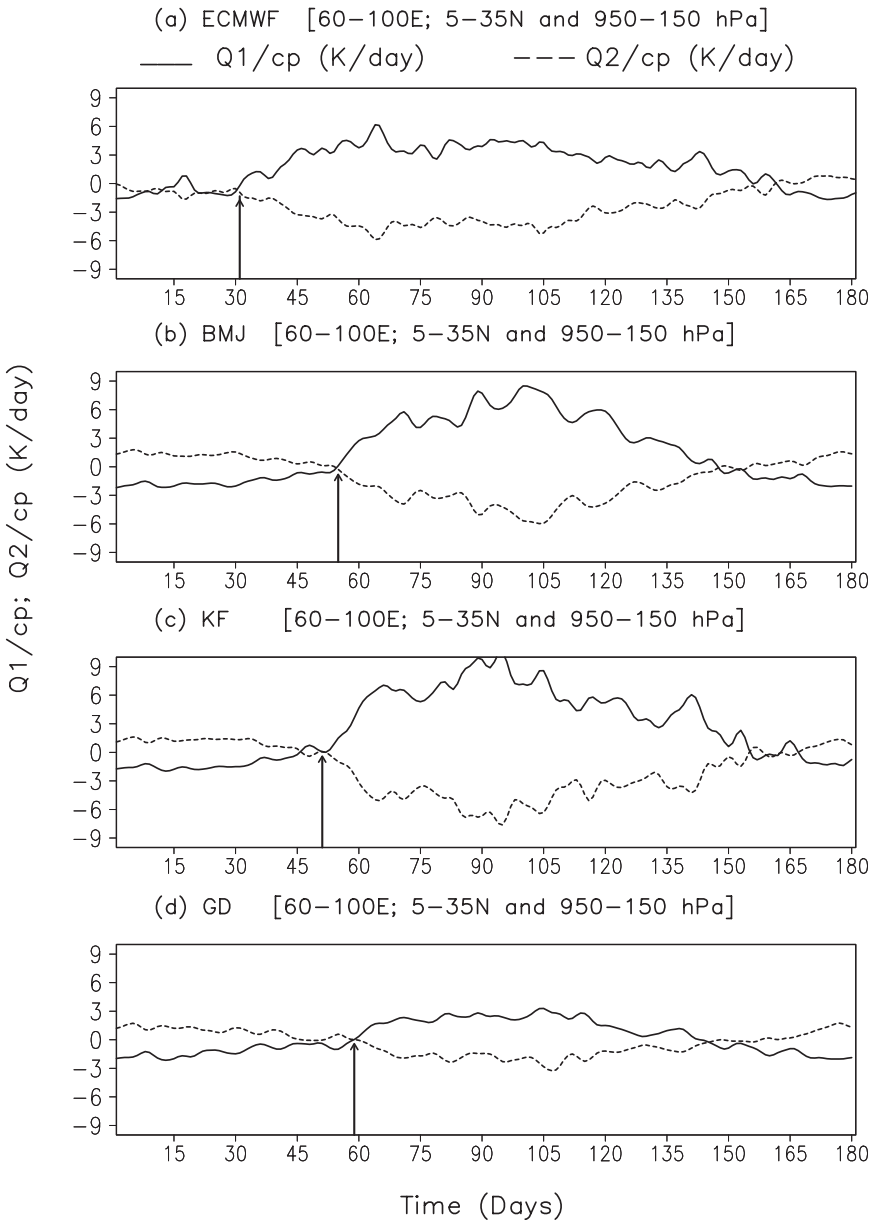

FIG. 14. Time evolutions (May–October) of the apparent heat source (solid, K day^{-1}), moisture sink (dotted, K day^{-1}) averaged over 5°–35°N, 60°–100°E for 2001–07 in (a) ECMWF, (b) BMJ, (c) KF, and (d) GD. The vertical integration is from 950 to 150 hPa. The onset dates are marked by arrows in each panel.

distributions of precipitation, apparent heat sources (Q_1), moisture sinks (Q_2), and moist static energies (MSEs) are analyzed to determine the thermodynamical reasons behind the deficiencies in the seasonal mean precipitation simulations. In this analysis, KF shows a stronger middle-tropospheric heating and GD consistently shows a weak middle-tropospheric heating, where only BMJ is closer to the observed profile of Q_1. The stronger (weaker) heating by KF (GD) in the middle troposphere could lead to stronger (weaker) upper-air divergence (also seen in the mean 200-hPa wind), which eventually can increase (decrease) lower-level convergence, resulting in enhanced (suppressed) updrafts that may finally lead to moist (dry) biases in the precipitation.

The analysis of the seasonal evolutions of Q_1 and Q_2 brings out the competition between the two important moist processes, namely evaporation and condensation. It is found that KF is unable to reproduce the domination

of evaporation over condensation at the time of withdrawal, indicating excess rain even at the end of the season, whereas GD shows a weak seasonal cycle of evaporation and condensation. This helps GD in producing the dry bias in the seasonal mean precipitation simulation. On the other hand, BMJ could realistically depict the domination of evaporation compared to condensation till mid-June. The enhancement of condensation over evaporation after the monsoon onset and followed by a maxima in July–August, as well as the reduction in condensation at the time of withdrawal, are only reasonably captured by BMJ.

Finally, it can be said that KF produces a stronger instability and intense updraft resulting in a large moist bias. GD, on the other hand, produces a weaker instability and weaker updraft, resulting in a relatively dry bias. The bias is mostly contributed from the moderate rain-rate category in the GD case and from the heavy rain-rate category in KF. BMJ also shows certain biases compared to the observations. The improvement in formulation that can give an accurate profile of Q_1 and Q_2, and remove the deficiency of producing the right PDF at the correct proportion, could result in a significant improvement in the precipitation bias in weather and climate applications of regional models.

Thus, the present study establishes the reasons behind the seasonal mean precipitation biases shown by different convection schemes. Further, it is demonstrated how the individual rain-rate categories contribute to the total bias of the seasonal mean. However, the reason behind the bias arising from different rain-rate categories remains to be explained and will be the subject of another study. This study is unique in the sense that it is the first time WRF is run at a high resolution (15 km) for a longer time (7 yr) over the Indian region to critically evaluate the reasons behind the precipitation biases and identify the deficiencies in the convective closures. In future studies, the BMJ convective parameterization, particularly the shallow and deep convective triggers, will be further modified to remove some of the deficiencies documented in this study.

Acknowledgments. Indian Institute of Tropical Meteorology, Pune, is fully funded by the Ministry of Earth Sciences, Government of India, New Delhi. The authors wish to thank the anonymous reviewers for their constructive comments, which have helped to improve the quality of the paper. They would also like to thank the National Centers for Environmental Prediction (NCEP) and the National Center for Atmospheric Research, as well as the NCEP/Marine Modeling and Analysis Branch (MMAB), for giving free access to their data. The authors are thankful to the European Centre for Medium-Range Weather Forecasts (ECMWF) for ERA interim data obtained from the ECMWF data server. The Mesoscale and Microscale Divisions of NCAR are sincerely acknowledged for online access to the Advanced Research Weather Research and Forecasting (WRF-ARW) model. The use of observed high-resolution rainfall data from the India Meteorological Department (IMD), Global Precipitation Climatology Project (GPCP), and Tropical Rainfall Measuring Mission (TRMM) are also acknowledged with thanks. The availability of the GrADS software used for preparing the diagrams is also thankfully acknowledged.

REFERENCES

Anthes, R. A., Y. H. Kuo, E. Y. Hsie, S. Low, and T. W. Bettge, 1989: Estimation of skill and uncertainty in regional numerical models. *Quart. J. Roy. Meteor. Soc.,* **115,** 763–806.

Bechtold, P., E. Bazile, F. Guichard, P. Mascart, and E. Richard, 2001: A mass-flux convection scheme for regional and global models. *Quart. J. Roy. Meteor. Soc.,* **127,** 869–886.

Betts, A. K., 1986: A new convective adjustment scheme. Part I: Observational and theoretical basis. *Quart. J. Roy. Meteor. Soc.,* **112,** 677–692.

——, and M. J. Miller, 1986: A new convective adjustment scheme. Part II: Single column tests using GATE wave, BOMEX, and arctic air-mass data sets. *Quart. J. Roy. Meteor. Soc.,* **112,** 693–709.

Bhaskaran, B., R. G. Jones, J. M. Murphy, and M. Noguer, 1996: Simulations of the Indian summer monsoon using a nested climate model: Domain size experiments. *Climate Dyn.,* **12,** 573–587.

Charney, J. G., and J. Shukla, 1981: Predictability of monsoons. *Monsoon Dynamics,* J. Lighthill and R. P. Pearce, Eds., Cambridge University Press, 99–109.

Das, S., A. K. Mitra, G. R. Iyengar, and S. Mohandas, 2001: Comprehensive test of different cumulus parameterization schemes for the simulation of Indian summer monsoon. *Meteor. Atmos. Phys.,* **78,** 227–244.

Dash, S. K., M. S. Shekhar, and G. P. Singh, 2006: Simulation of Indian summer monsoon circulation and rainfall using RegCM3. *Theor. Appl. Climatol.,* **86,** 161–172.

DeMott, C. A., D. A. Randall, and M. Khairoutdinov, 2007: Convective precipitation variability as a tool for general circulation model analysis. *J. Climate,* **20,** 91–112.

Dudhia, J., 1989: Numerical study of convection observed during the Winter Monsoon Experiment using a mesoscale two-dimensional model. *J. Atmos. Sci.,* **46,** 3077–3107.

Gallus, W. A., Jr., 1999: Eta simulations of three extreme precipitation events: Sensitivity to resolution and convective parameterization. *Wea. Forecasting,* **14,** 405–426.

Giorgi, F., and L. O. Mearns, 1991: Approaches to the simulation of regional climate change: A review. *Rev. Geophys.,* **29,** 191–216.

——, C. Shields Brodeur, and G. T. Bates, 1994: Regional climate change scenarios over the United States produced with a nested regional climate model. *J. Climate,* **7,** 375–399.

Grell, G. A., and D. Devenyi, 2002: A generalized approach to parameterizing convection combining ensemble and data assimilation techniques. *Geophys. Res. Lett.,* **29,** 1693, doi:10.1029/2002GL015311.

Im, E.-S., E.-H. Park, W.-T. Kwon, and F. Giorgi, 2006: Present climate simulations over Korea with a regional climate model using a one-way double-nested system. *Theor. Appl. Climatol.,* **86,** 187–200.

——, J.-B. Ahn, A. R. Remedio, and W.-T. Kwon, 2008: Sensitivity of the regional climate of East/Southeast Asia to convective parameterizations in the RegCM3 modelling system. Part 1: Focus on the Korean peninsula. *Int. J. Climatol.,* **28,** 1861–1877, doi:10.1002/joc.1664.

Jacob, D., and R. Podzum, 1997: Sensitivity studies with the regional climate model REMO. *Meteor. Atmos. Phys.,* **63,** 119–129.

Janjić, Z. I., 1994: The step-mountain eta coordinate model: Further developments of the convection, viscous sublayer, and turbulence closure schemes. *Mon. Wea. Rev.,* **122,** 927–945.

Jha, B., T. N. Krishnamurti, and Z. Christides, 2000: A note on horizontal resolution dependence for monsoon rainfall simulations. *Meteor. Atmos. Phys.,* **74,** 11–17.

Jones, R. G., J. M. Murphy, and M. Noguer, 1995: Simulation of climate change over Europe using a nested regional climate model. Part I: Assessment of control climate, including sensitivity to location of lateral boundaries. *Quart. J. Roy. Meteor. Soc.,* **121,** 1413–1449.

Kain, J. S., 2004: The Kain–Fritsch convective parameterization: An update. *J. Appl. Meteor.,* **43,** 170–181.

——, and J. M. Fritsch, 1993: Convective parameterization for mesoscale models: The Kain–Fritsch scheme. *The Representation of Cumulus Convection in Numerical Models, Meteor. Monogr.,* No. 46, Amer. Meteor. Soc., 165–170.

Kalnay, E., and Coauthors, 1996: The NCEP/NCAR 40-Year Reanalysis Project. *Bull. Amer. Meteor. Soc.,* **77,** 437–471.

Kang, I.-S., and J. Shukla, 2005: Dynamical seasonal prediction and predictability of monsoon. *The Asian Monsoon,* B. Wang, Ed., Praxis, 585–612.

——, J.-Y. Lee, and C.-K. Park, 2004: Potential predictability of summer mean precipitation in a dynamical seasonal prediction system with systematic error correction. *J. Climate,* **17,** 834–844.

Kumar, K. K., M. Hoerling, and B. Rajagopalan, 2005: Advancing dynamical prediction of Indian monsoon rainfall. *Geophys. Res. Lett.,* **32,** L08704, doi:10.1029/2004GL021979.

Lee, D.-K., and M.-S. Suh, 2000: Ten year east Asian summer monsoon simulation using a regional climate model (RegCM2). *J. Geophys. Res.,* **105,** 29 565–29 577.

Lin, Y.-L., R. D. Farley, and H. D. Orville, 1983: Bulk parameterization of the snow field in a cloud model. *J. Climate Appl. Meteor.,* **22,** 1065–1092.

Liu, C., and M. W. Moncrieff, 2007: Sensitivity of cloud-resolving simulations of warm season convection to cloud microphysics parameterizations. *Mon. Wea. Rev.,* **135,** 2854–2868.

Martin, G. M., and M. K. Soman, 2000: Effects of changing physical parameterization schemes on the simulation of the Asian summer monsoon in the UK Met Office unified model. Hadley Centre Tech. Note HCTN17, 48 pp.

Mlawer, E. J., S. J. Taubman, P. D. Brown, M. J. Iacono, and S. A. Clough, 1997: Radiative transfer for inhomogeneous atmosphere: RRTM, a validated correlated-k model for the long-wave. *J. Geophys. Res.,* **102** (D14), 16 663–16 682.

Monin, A. S., and A. M. Obukhov, 1954: Basic laws of turbulent mixing in the surface layer of the atmosphere (in Russian). *Contrib. Geophys. Inst. Acad. Sci. USSR,* **151,** 163–187.

Noh, Y., W. G. Cheon, S.-Y. Hong, and S. Raasch, 2003: Improvement of the K-profile model for the planetary boundary layer based on large eddy simulation data. *Bound.-Layer Meteor.,* **107,** 401–427.

Rajeevan, M., J. Bhate, J. D. Kale, and B. Lal, 2006: High resolution daily gridded rainfall data for the Indian region: Analysis of break and active monsoon spells. *Curr. Sci.,* **91,** 293–306.

Rajendran, K., and A. Kitoh, 2008: Indian summer monsoon in future climate projection by a super high resolution global model. *Curr. Sci.,* **95,** 1560–1569.

——, R. S. Nanjundiah, and J. Srinivasan, 2002: Comparison of seasonal and intraseasonal variation of tropical climate in NCAR CCM2 GCM with two different cumulus schemes. *Meteor. Atmos. Phys.,* **79,** 57–86.

Randall, D. A., and Coauthors, 2007: Climate models and their evaluation. *Climate Change 2007: The Physical Science Basis,* S. Solomon et al., Eds., Cambridge University Press, 591–662.

Ratnam, J. V., and K. K. Kumar, 2005: Sensitivity of the simulated monsoons of 1987 and 1988 to convective parameterization schemes in MM5. *J. Climate,* **18,** 2724–2743.

Schumacher, C., and R. A. Houze Jr., 2003: Stratiform rain in the tropics as seen by the TRMM Precipitation Radar. *J. Climate,* **16,** 1739–1756.

Shukla, J., 1981: Dynamical predictability of monthly means. *J. Atmos. Sci.,* **38,** 2547–2572.

Skamarock, W. C., J. B. Klemp, J. Dudhia, D. O. Gill, D. M. Barker, W. Wang, and J. G. Powers, 2005: A description of the Advanced Research WRF version 2. NCAR Tech. Note NCAR/TN-468STR, 88 pp.

Sperber, K. R., S. Hameed, G. L. Potter, and J. S. Boyle, 1994: Simulation of northern summer monsoon in the ECMWF model: Sensitivity to horizontal resolution. *Mon. Wea. Rev.,* **122,** 2461–2481.

Thiebaux, J., E. Rogers, W. Wang, and B. Katz, 2003: A new high-resolution blended real-time global sea surface temperature analysis. *Bull. Amer. Meteor. Soc.,* **84,** 645–656.

Vernekar, A. D., and Y. Ji, 1999: Simulation of the onset and intraseasonal variability of two contrasting summer monsoons. *J. Climate,* **12,** 1707–1725.

Wang, W., and N. L. Seaman, 1997: A comparison study of convective parameterization schemes in a mesoscale model. *Mon. Wea. Rev.,* **125,** 252–278.

Xavier, P. K., C. Marzin, and B. N. Goswami, 2007: An objective definition of the Indian summer monsoon season and a new perspective of ENSO–monsoon relationship. *Quart. J. Roy. Meteor. Soc.,* **133,** 749–764.

Yanai, M., S. Esbensen, and J. Chu, 1973: Determination of the bulk properties of tropical cloud clusters from large heat and moisture budgets. *J. Atmos. Sci.,* **30,** 611–627.